Percolation in random sequential adsorption of mixtures on a triangular lattice

D Dujak[1], A Karač[2], Lj Budinski-Petković[3], I Lončarević[3], Z M Jakšić[4] and S B Vrhovac[4]

[1] Faculty of Metallurgy and Technology, University of Zenica, Zenica, Bosnia and Herzegovina
[2] Polytechnic Faculty, University of Zenica, Zenica, Bosnia and Herzegovina
[3] Faculty of Engineering, Trg D. Obradovića 6, Novi Sad 21000, Serbia
[4] Institute of Physics, Belgrade, University of Belgrade, Pregrevica 118, Zemun 11080, Belgrade, Serbia

E-mail: ivanalon@uns.ac.rs

Abstract. Percolation properties of two-component mixtures are studied by Monte Carlo simulations. Objects are deposited onto a substrate according to the random sequential adsorption model. Various shapes making the mixtures are made by self-avoiding walks on a triangular lattice. Percolation threshold θ_p for mixtures of objects covering the same number of sites is always lower than θ_p for the more compact object, and it can be even lower than θ_p for both components. Mixtures of percolating and non-percolating objects almost always percolate, but the percolation threshold is higher than θ_p for the percolating component. Adding a shape of high connectivity to a system of compact non-percolating objects, makes the deposit percolate. Lowest percolation thresholds are obtained for mixtures with elongated angled objects. Dependence of θ_p on the object length exhibits a minimum, so it could be estimated that the angled objects of length $6 \leqslant \ell \leqslant 10$ give the largest contribution to the percolation.

Keywords: numerical simulations, percolation problems

Contents

1. Introduction

Irreversible deposition or random sequential adsorption (RSA) model has a wide range of applications in biology, nanotechnology, material science and even some ecological and sociological problems. Depending on the problem of interest, depositing objects can be various macromolecules, proteins, DNA segments, polymer chains, nanotubes, colloidal particles etc [1–4]. If the relaxation times are much longer than the deposit formation, adsorption of these objects can be modeled by irreversible deposition of various shapes on a lattice or continuum substrate.

In RSA models particles are randomly, sequentially and irreversibly deposited onto a substrate. The particles are not allowed to overlap, so the dominant effect in RSA is the blocking of the available substrate area and the limiting (jamming) θ_{jam} coverage is less than in close packing. The kinetic properties of a deposition process are described by the time evolution of the coverage $\theta(t)$, that is the fraction of the substrate area occupied by the adsorbed particles [5–7].

Depending on the studied system, the substrate can be continuum or discrete, and RSA models can differ in substrate dimensionality. Exact solutions are available only for a number one-dimensional problems [8, 9]. Due to the complexity of the geometrical exclusion effects in two and three dimensions, Monte Carlo simulations are one of the primary investigating tools for these deposition processes [10–15].

The long-term behavior of the coverage fraction $\theta(t)$ is known to be algebraic for continuum systems [2, 11] and exponential for lattice models [12, 14]. For discrete substrates the late time kinetics of the process is described by the time dependence:

$$\theta(t) = \theta_{jam} - A e^{-t/\tau}, \tag{1}$$

where A and τ are parameters that depend on the shape, orientational freedom of the objects, and on the dimensionality of the substrate.

During the process of irreversible deposition, coverage increases causing the growth of clusters of occupied sites. Percolation assumes the formation of a large cluster that connects two opposite sides of the substrate [16]. The interplay between RSA and percolation has been discussed in several works [17–19]. Motivated by irreversible deposition of large particles, such as polymers, the temperature behavior of the percolation

threshold of adsorbed flexible chains was studied in [20]. Percolation properties of flexible chains were discussed in [21] for the square and for the triangular lattice. Simulations were performed for various chain lengths and the compositions that give minimum percolation thresholds were identified. For longer and more bent chains non-percolation regime was observed. Results for the percolation thresholds, jamming coverages and their ratios for deposition of various objects on a triangular lattice were presented in [22]. Depositing objects of various shapes were made by self-avoiding random walks on the lattice. It was found that the percolation threshold monotonically decreases for elongated shapes and increases for more compact objects with the object size. For compact objects of larger sizes jamming coverage was reached before the percolation.

Percolation has also been studied in the presence of defects on a lattice [23, 24]. For each object shape there is a concentration of defects above which percolation cannot be achieved. Generally, the critical defect concentration has higher values for objects forming more porous surface configurations, and lower values for compact objects.

Existence of percolation is relevant for many physical, chemical and biological phenomena. Particle transport in overcrowded media, such as dense colloidal suspensions, supercooled liquids, diffusion of proteins in crowded environment of nucleic acids and other macromolecules, is highly affected by the density of obstacles. In [25] it has been shown that anomalous diffusion sets on when the obstacles reach the percolation threshold.

Polydispersity is a common feature of real physical systems. There are numerous studies of irreversible deposition of mixtures, including binary mixtures [26, 27], as well as polydisperse mixtures [28]. Reversible RSA of mixtures on a triangular lattice has also been studied [29]. Motivated by a broad application of the results for percolations in various systems, we present the results for percolation in irreversible deposition of binary mixtures. Depositing objects are made by self-avoiding random walks on a triangular lattice.

The paper is organized as follows. Section 2 describes the details of the model and simulations. Results and discussions are given in section 3, while section 4 contains some additional comments and final remarks.

2. Definition of the model and the simulation method

Depositing objects of various shapes are made by self-avoiding walks on a triangular lattice. Binary mixtures are composed of the objects shown in tables 1–3. The Monte Carlo simulations are performed on a triangular lattice of size up to $L = 3200$. For the approach to the jamming coverage, periodic boundary conditions are used in all directions. On the other hand, when studying percolation, hard boundary conditions are used in the horizontal direction, in which the onset of percolation is detected, and periodic boundary conditions in the other two directions.

At each Monte Carlo step a lattice site is selected at random. If the selected site is unoccupied, one of the objects making the mixture is chosen uniformly at random and deposition of the selected object is tried in one of the six orientations. We fix the

beginning of the walk that makes the shape at the selected site and search whether all successive ℓ sites are unoccupied. If so, we occupy these $\ell + 1$ sites and place the object. If the attempt fails, a new site and a depositing object is selected at random. The jamming limit is reached when neither of the objects can be placed in any position on the lattice.

The time is counted by the number of attempts to select a lattice site and scaled by the total number of lattice sites. In all the simulations the data are averaged over 500 independent runs.

In this work we concentrate on the study of percolation in irreversible deposition of binary mixtures. The coverage of the surface is increased in the RSA process up to the percolation threshold, when there appears a cluster that extends through the whole system—from the left to the right side of the lattice. The tree-based union/find algorithm is used to determine the percolation threshold [30]. Each cluster of connected sites is stored as a separate tree, having a single 'root' site. All sites of the cluster possess pointers to the root site, so it is simple to ascertain whether two sites are members of the same cluster. When a deposited object connects two separate clusters, they are amalgamated by adding a pointer from the root of the smaller cluster to the root of the larger one. This procedure is repeated until the percolation threshold is reached, i.e. until the opposite sides of the lattice are connected by a single cluster.

3. Results and discussion

Jamming coverages and percolation thresholds were first determined for the objects given in table 1. It is important to note that a walk of length ℓ always covers $\ell + 1$ lattice site. Analyzing the three representative sets of lengths $\ell = 2, 3$, and 6, we can see that the percolation threshold for the objects covering the same number of sites has the lowest value for the elongated shapes containing an obtuse angle (in further text referred to as the angled objects). On the other hand, compact objects, such as triangles, rhombuses and hexagons, have a lower connecting probability and higher values of the percolation thresholds. The number of nearest neighbors m seems to be a quantity that is closely related to the connectivity, and it is included in table 1. It can be seen that the percolation threshold decreases with m for objects of the same length. These conclusions were driven from simulations performed for a large variety of objects [22].

The effective percolation threshold θ_p (measured for a finite lattice) approaches the asymptotic value θ_p^* ($L \to \infty$) via the power law:

$$\theta_p - \theta_p^* \propto L^{-1/\nu} . \tag{2}$$

The theoretical value for the critical exponent is $\nu = 4/3$ for two-dimensional systems. Simulations were performed for the lattice size ranging from $L = 200$ to $L = 3200$ for the mixtures $(B) + (C)$, $(E) + (K)$ and $(T) + (S)$. Plots of the mean value of θ_p obtained for various lattice sizes against $L^{-1/\nu}$, shown in figure 1, confirm the validity of the finite-size scaling. Although θ_p is sensitive to the lattice size L, the asymptotic value of the percolation threshold θ_p^* coincides with the value of θ_p obtained for the largest lattice, within the limits of the statistical error. Thus, results for a sufficiently large

Table 1. Samples of depositing objects (x), with m nearest neighbors and of length $\ell^{(x)}$. The jamming coverages θ_{jam} and the percolation thresholds θ_p are given for the illustration of their percolation properties. The numbers in parentheses are the numerical values of the standard uncertainty of $\theta_{\text{jam}}^{(x)}$ and $\theta_p^{(x)}$ referred to the last digits of the quoted value.

(x)	Shape	m	$\ell^{(x)}$	$\theta_{\text{jam}}^{(x)}$	$\theta_p^{(x)}$
(A)		8	1	0.9139(5)	0.4841(13)
(B)		10		0.8362(7)	0.4611(9)
(C)		10	2	0.8345(8)	0.4585(11)
(D)		9		0.7970(4)	0.5214(9)
(E)		12		0.7886(8)	0.4399(12)
(F)		12	3	0.7653(10)	0.4304(12)
(K)		10		0.7593(4)	0.5387(6)
(S)		18		0.7212(7)	0.4145(17)
(T)		12	6	0.6696(8)	0.5843(13)
(R)		18		0.6445(10)	0.3831(14)
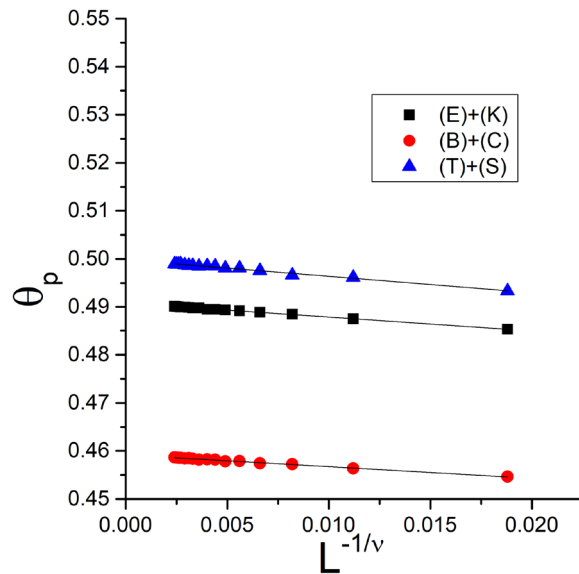
Figure 1. Finite-size scaling of the mean value of the percolation threshold θ_p against $L^{-1/\nu}$ for the mixtures $(B) + (C)$, $(E) + (K)$ and $(T) + (S)$ (see table 2). Straight lines represent linear fit of the form $\theta_p = \theta_p^* + L^{-1/\nu}$, where the asymptotic value of the percolation threshold θ_p^* coincides with the value θ_p obtained for the largest lattice, within the statistical error.

lattice can be taken instead of the asymptotic value θ_p^*. The similar method was used in [23]. For further analysis of the percolation threshold of mixtures we take the results for $L = 3200$.

According to the scaling theory, the standard deviation σ_p of the percolation threshold measured for a finite lattice L satisfies the power law
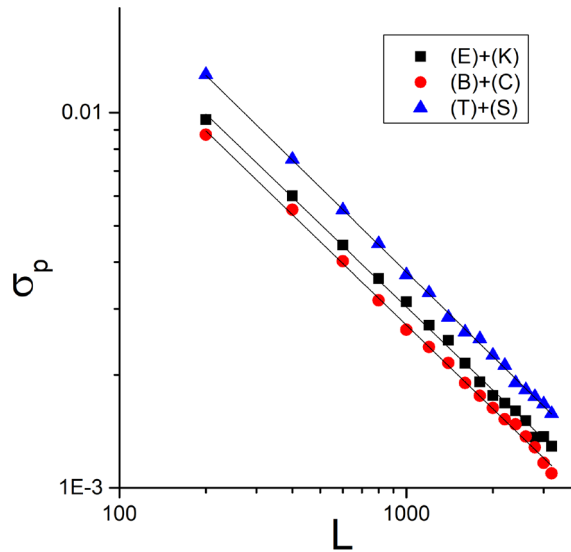
Figure 2. Finite-size scaling of the standard deviation σ_p against L for the mixtures $(B) + (C)$, $(E) + (K)$ and $(T) + (S)$ (see table 2).
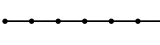
$$\sigma_p \propto L^{-1/\nu} \,. \tag{3}$$

Scaling of the standard deviation σ_p is ilustrated for the mixtures $(B) + (C)$, $(E) + (K)$ and $(T) + (S)$ in figure 2. The values of σ_p are shown versus L on a log–log scale and they lie on parallel straight lines. The slope of the lines corresponds to the exponent $1/\nu = 0.74 \pm 0.01$.

In order to gain an insight into the way the combinations of object shapes affects the percolation properties, simulations were performed for the mixtures of objects covering the same number of lattice sites, shown in table 2. We can see that the value of θ_p of a mixture is either between the values for the mixture components, or lower than the percolation thresholds for both shapes making the mixture, due to the high connectivity of both mixture components.

Results are also obtained for larger sizes of the basic objects shown in table 3. Larger elongated objects, k-mers and angled objects, are made by repeating each step of the basic shape the same number of times. Compact objects of larger sizes, triangles, rhombuses and hexagons, occupy all comprised sites on the lattice. Jamming coverage decreases with the object size for all objects shapes. On the other hand, for the elongated angled object percolation threshold θ_p decreases with their size, but increases for the compact ones [22]. In table 4 jamming coverages and percolation thresholds are given for triangles, rhombuses and hexagons of various sizes. Values of the jamming coverages decrease, while the percolation thresholds increase with the object size and for larger objects jamming coverage is reached before the percolation. For the most compact object, hexagon, percolation is possible only for the basic shape.

It is interesting to examine the behavior of mixtures of percolating and non-percolating objects. In table 5 results are given for a large number of combinations of objects of various shapes and sizes. Notations in the table 5 coincide with those from tables 1–4 for triangles, K for rhombuses and T for hexagons. The index number stands for the number of steps of the walk making the shape. For mixtures of two non-percolating

Table 2. Jamming $\theta_{\mathrm{jam}}^{(x+y)}$ and and percolation threshold $\theta_p^{(x+y)}$ for the binary mixtures composed of the objects of the same length ℓ. The numbers in parentheses are the numerical values of the standard uncertainty of $\theta_{\mathrm{jam}}^{(x+y)}$ and $\theta_p^{(x+y)}$ referred to the last digits of the quoted value.

$(x+y)$	Shape	ℓ	$\theta_{\mathrm{jam}}^{(x+y)}$	$\theta_p^{(x+y)}$
$(B+C)$	⊶ + ╱		0.8525(7)	0.4587(12)
$(B+D)$	⊶ + ╲	2	0.8588(6)	0.4926(12)
$(C+D)$	╱ + ╲		0.8625(7)	0.4910(12)
$(E+K)$	⊶⊶ + ⊐		0.8107(8)	0.4901(13)
$(E+F)$	⊶⊶ + ⊿	3	0.7878(9)	0.4350(11)
$(K+F)$	⊐ + ⊿		0.8141(7)	0.4875(12)
$(T+S)$	⬭ + ⊶⊶⊶		0.7125(7)	0.4991(16)
$(T+R)$	⬭ + ⊶⊶╱	6	0.7089(8)	0.4919(15)

Table 3. Basic shapes used for the construction of objects of larger sizes.

Shape	$\ell^{(x)}$
⊶	1
╱	2
╲	2
⊐	3
⬭	6

objects percolation was never reached. On the contrary, mixtures containing one percolating object, even if it is a compact one, and one non-percolating object, exhibit percolation. In the latter case the percolation threshold for the mixture is always larger than θ_p for the percolating object. Adding non-percolating objects to the system of percolating ones, makes the connecting of the objects on the lattice more difficult and percolation sets in at larger values of coverage fractions.

Mixtures were made of non-percolating objects and objects with better connectivity that easily reach percolation. Simulations were performed for the mixtures of k-mers of various lengths and the non-percolating triangles, rhombuses and hexagons denoted as $(D_{20}), (D_{27}), (K_{15}), (K_{24}), (T_{18})$, and (T_{36}). The percolation threshold θ_p and the jamming limit θ_{jam}, as well as their ratio $\theta_p/\theta_{\mathrm{jam}}$, are plotted versus the length of the k-mer combined with the mentioned non-percolating objects in figure 3. It can be seen that the jamming coverage monotonically decreases with the length ℓ of the k-mers, while the percolation threshold decreases for shorter k-mers, reaches a minimum and slightly increases for longer k-mers. The ratio $\theta_p/\theta_{\mathrm{jam}}$ increases for all the mixtures. As expected, the highest values of θ_p are obtained for the mixtures containing the larger hexagon (T_{36}), and a little lower for the smaller hexagon (T_{18}) (see, figure 4). Values of θ_p for (K_{24}) and (D_{27}) and also for (K_{15}) and (D_{20}) are intertwined when varying the

Table 4. Values of the jamming coverages and the percolation thresholds for compact objects of larger sizes. For larger sizes of compact objects a no-percolation regime is observed.

| (x_ℓ)	Shape	$\ell^{(x)}$	$\theta_{\mathrm{jam}}^{(x)}$	θ_p
(D_2)		2	0.7970(4)	0.5214(9)
(D_5)		5	0.7211(5)	0.5524(14)
(D_9)		9	0.6816(6)	0.5789(15)
(D_{14})	· · ·	14	0.6572(6)	0.6003(5)
(D_{20})	· · ·	20	0.6406(8)	/
(D_{27})	· · ·	27	0.6286(7)	/
(K_3)		3	0.7591(4)	0.5393(12)
(K_8)		8	0.6793(6)	0.5793(14)
(K_{15})	· · ·	15	0.6428(7)	/
(K_{24})	· · ·	24	0.6220(7)	/
(T_6)		6	0.6696(5)	0.5843(13)
(T_{18})		18	0.6148(6)	/
(T_{36})	· · ·	36	0.5942(8)	/

Table 5. Values of the percolation thresholds for mixtures of one percolating x_ℓ and one non-percolating object y_ℓ.

$(x_\ell + y_\ell)$	$\theta_p^{(x)}$, $\theta_p^{(y)}$	θ_p^{x+y}
$(D_2 + D_{20})$	0.5214(9), no	0.5646(14)
$(D_2 + D_{27})$	0.5214(9), no	0.5699(13)
$(D_5 + D_{20})$	0.5524(14), no	0.5805(15)
$(D_5 + D_{27})$	0.5524(14), no	0.5858(15)
$(D_9 + D_{20})$	0.5789(15), no	0.5977(18)
$(D_9 + D_{27})$	0.5789(15), no	0.6035(18)
$(D_{14} + D_{20})$	0.6003(5), no	0.6109(17)
$(D_{14} + D_{27})$	0.6003(5), no	0.6196(19)
$(K_3 + K_{15})$	0.5393(12), no	0.5715(14)
$(K_3 + K_{24})$	0.5393(12), no	0.5805(14)
$(K_8 + K_{15})$	0.5793(14), no	0.5927(15)
$(K_8 + K_{24})$	0.5793(14), no	0.6036(15)
$(K_3 + D_{20})$	0.5393(12), no	0.5726(13)
$(K_3 + D_{27})$	0.5393(12), no	0.5780(14)
$(K_8 + D_{20})$	0.5793(14), no	0.5971(16)
$(K_8 + D_{27})$	0.5793(14), no	0.6025(15)
$(D_2 + K_{15})$	0.5214(9), no	0.5641(13)
$(D_{14} + K_{15})$	0.6003(5), no	0.6051(6)
$(D_{14} + K_{24})$	0.6003(5), no	0.6202(17)
$(T_6 + T_{18})$	0.5843(13), no	0.6110(14)
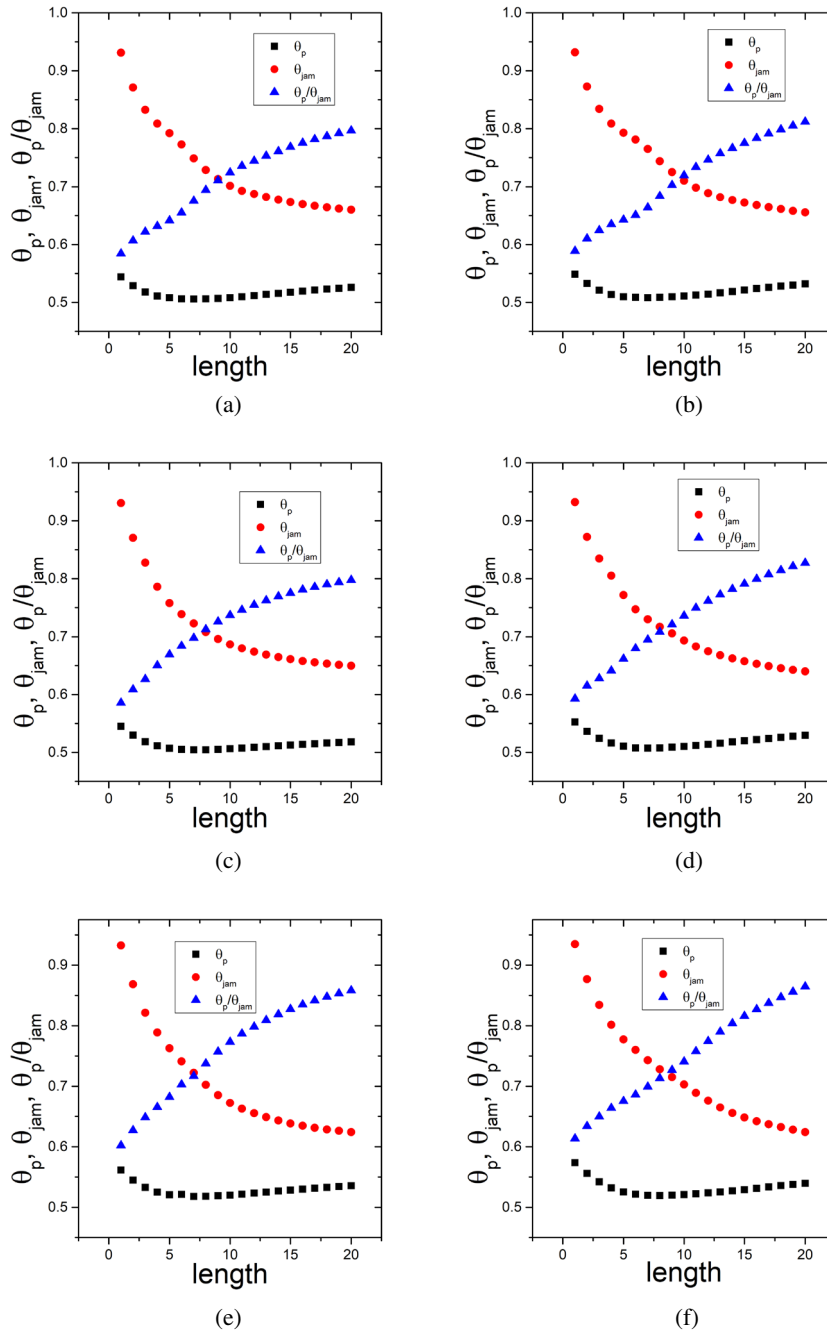
Figure 3. Dependence of the percolation threshold θ_p, the jamming coverage θ_{jam} and their ratio $\theta_p/\theta_{\text{jam}}$ on the length of k-mer combined with non-percolating object: (a) triangle (D_{20}), (b) triangle (D_{27}), (c) rhombus (K_{15}), (d) rhombus (K_{24}), (e) hexagon (T_{18}) and (f) (T_{36}).

length of the *k*-mer as the second component of the mixture. For sufficiently short *k*-mers percolation threshold for mixtures with objects (D_{27}) and (D_{20}) are below the thresholds for mixtures with objects (K_{24}) and (K_{15}), respectively. For longer *k*-mers, the inversion of percolation thresholds for these mixtures occurs. This means that in the case of mixtures with shorter *k*-mers percolation is reached more easily when the
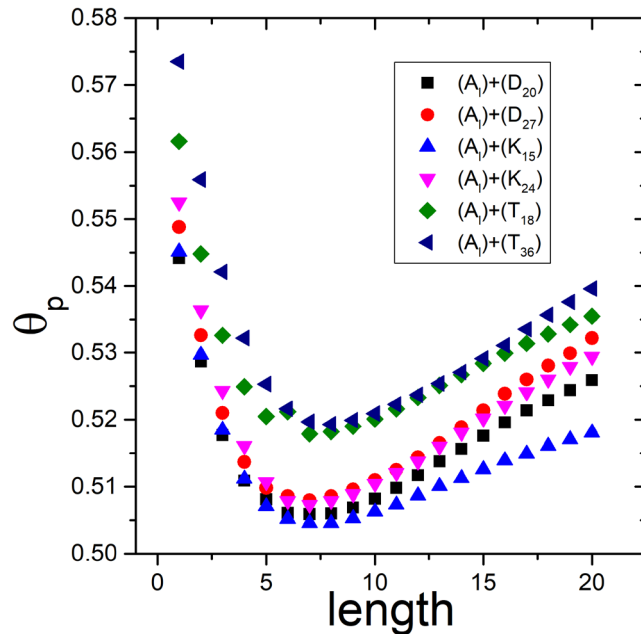
Figure 4. Dependance of the percolation threshold θ_p on the length of k-mer for the various mixtures made of k-mers and non-percolating triangles, rhombuses and hexagons, as indicated in the legend.

second component is a triangle, and for longer k-mers the situation is inverse, percolation is favored for the mixtures with rhombuses. A striking feature of the plots shown in figure 4 is that the minimum θ_p is obtained for the same value of the k-mer length, $\ell = 7$, regardless of the second mixture component. It should be mentioned that the obtained minimum is broad, with the values of θ_p for the k-mers differing in one lattice spacing being within the statistical error.

In addition, results were obtained for the mixtures of angled objects (C_l) of various sizes and the non-percolating objects $(D_{20}), (D_{27}), (K_{15}), (K_{24}), (T_{18})$, and (T_{36}). Corresponding plots of θ_p, θ_{jam} and $\theta_p/\theta_{\text{jam}}$ are shown in figure 5. These plots look similar to those for the mixtures of k-mers of various lengths and the chosen compact objects. The jamming coverage monotonically decreases, and the percolation threshold exhibits a minimum. Figure 6 shows the impact of the compact (non-percolating) object shape on the percolation threshold of the mixture. Values of θ_p for the mixtures of non-percolating objects and angled objects are even more intertwined than in the case of mixtures with k-mers. For most of the examined lengths of the angled objects, θ_p has largest values when the other component of the mixture are hexagons (T_{36}) for shorter (C_l), and (T_{18}) for longer ones. The lowest values of θ_p are obtained for the combinations of triangles and angled objects, with the component (D_{20}) for shorter (C_l), and with (D_{27}) for the longer angled objects. Similarly as in the case of k-mers of various lengths, these plots exhibit a minimum. For most of the examined mixtures the minimum values of the percolation threshold are reached for $\ell = 8$, but for the combination ($C_l + K_{15}$) it is shifted to $\ell = 6$. For the mixture ($C_l + T_{36}$) containing the larger hexagon, the object with the lowest connectivity of all examined objects, the minimum of θ_p is obtained for $\ell = 10$. Increasing the length of the percolating object combined with a non-percolating one, the percolation threshold decreases, reaches a minimum value and
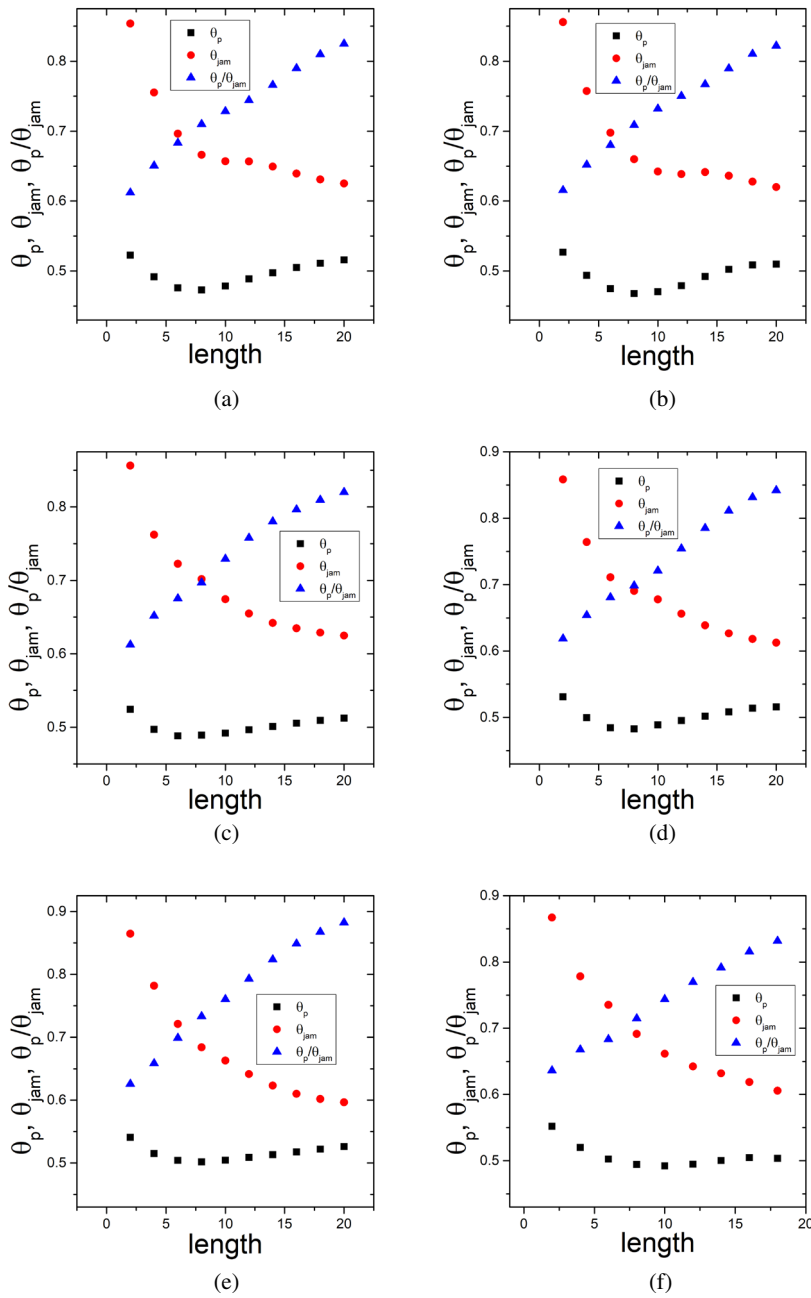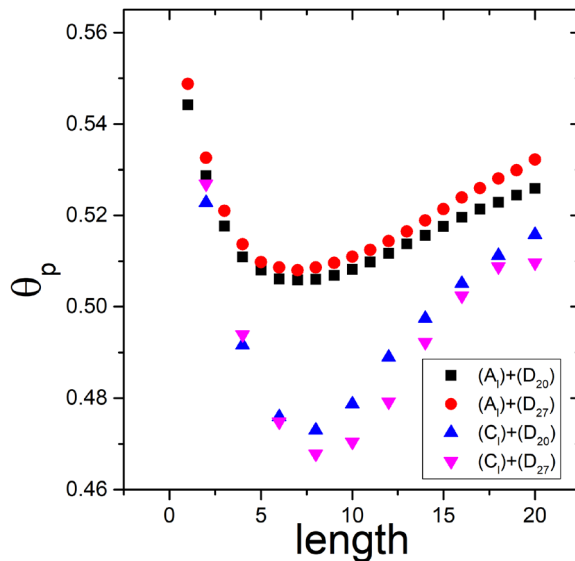
Figure 5. Dependence of the percolation threshold θ_p, the jamming coverage θ_{jam} and their ratio $\theta_p/\theta_{\mathrm{jam}}$ on the length of angled object (C_l) combined with non-percolating object: (a) triangle (D_{20}), (b) triangle (D_{27}), (c) rhombus (K_{15}), (d) rhombus (K_{24}), (e) hexagon (T_{18}) and (f) (T_{36}).

increases for longer percolating objects. Decrease of θ_p for shorter percolating objects is due to the increase of the surface porosity with ℓ. On the other hand, in the case of mixtures of non-percolating objects and longer percolating objects it is more difficult to reach the percolation, and θ_p increases with ℓ of the percolating component, getting closer to the jamming coverage.
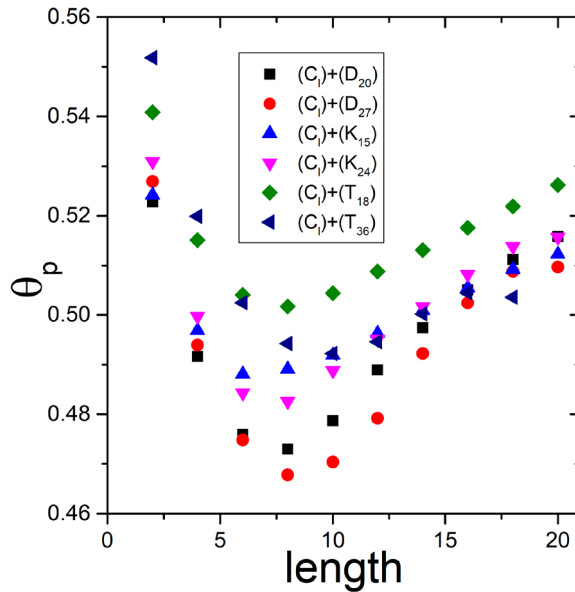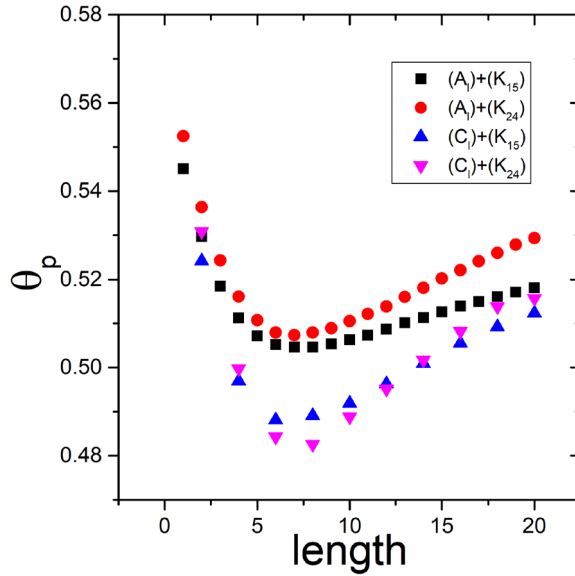
Figure 6. Dependance of the percolation threshold θ_p on the length of angled object (C_l) for the various mixtures made of angled objects (C_l) and non-percolating objects, as indicated in the legend.
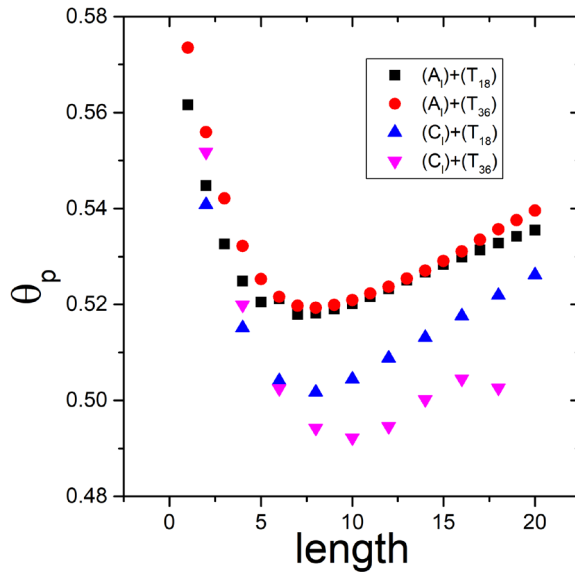

Figure 7. Dependance of the percolation threshold θ_p on the length of k-mer/angled object for the mixtures of k-mers and angled objects with triangles of two sizes D_{20} and D_{27}.

Let us now compare the percolation thresholds for the mixtures consisting of certain non-percolating objects and k-mers with those with angled objects instead of k-mers. In figure 7 plots are given for the mixtures of k-mers and angled objects of various lengths with triangles of two sizes: (D_{20}) and (D_{27}). We can see that the percolation is favored for the mixtures containing angled objects, in comparison to the mixtures with k-mers of various lengths. Similar plots are shown in figures 8 and 9 for the mixtures of rhombuses and hexagons with k-mers and angled objects of various lengths. Generally,

Figure 8. Dependance of the percolation threshold θ_p on the length of k-mer/ angled object for the mixtures of k-mers and angled objects with rhombuses of two sizes K_{15} and K_{24}.

Figure 9. Dependance of the percolation threshold θ_p on the length of k-mer/ angled object for the mixtures of k-mers and angled objects with hexagons of two sizes T_{18} and T_{36}.

percolation sets in more easily in combinations with angled objects. It should be noted that in the case of the mixture of the larger hexagon and the angled object of length $\ell = 20$, percolation is not reached. This is the consequence of the enhanced blocking of the substrate area in this case. On the other hand, for the mixture $C_{18} + T_{36}$ percolation threshold has lower value than for $C_{16} + T_{36}$, due to the more pronounced porosity of the surface in the case of longer angled object. It is interesting that for the mixtures

containing angled objects lower values of θ_p are obtained for larger sizes of the non-percolating component.

All these results suggest that mixtures of objects of higher and lower percolating thresholds show better percolating performance than the object that reaches percolation at higher coverages. Moreover, adding percolating objects with good connectivity to a system of non-percolating objects, makes the deposit percolate. It seems that the best connectivity is obtained for elongated, but angled objects that can make paths through various geometries of vacant sites.

4. Concluding remarks

Percolation phenomena have been investigated for a wide variety of binary mixtures by Monte Carlo simulations. Depositing objects were made by self-avoiding lattice steps on a triangular lattice and irreversibly placed on the substrate.

For the mixtures of object shapes covering the same number of sites it was found that the percolation threshold for mixtures is always lower than θ_p for the more compact object. When objects of high connectivity are combined, it can be even lower than θ_p for both components.

Mixtures of percolating and non-percolating objects almost always percolate, but the percolation threshold is higher than θ_p for the percolating component. Adding a component with good percolating properties to a system of non-percolating objects makes the resulting deposit percolate. For example, mixtures of k-mers and compact non-percolating objects exhibit percolation, and θ_p reaches a minimum value for the k-mer of length $\ell = 7$. Elongated angled objects have the lowest percolation thresholds, due to the porosity of the surface. In combinations with non-percolating objects they also give the lowest percolation thresholds of all investigated objects. A minimum of θ_p for the examined mixtures was obtained for $6 \leqslant \ell \leqslant 10$.

Thus, percolation of a deposit can be enhanced by adding a component with better percolating properties. Further investigations could be focused on percolation of mixtures with various fractional concentrations of mixture components, as well as on the percolation properties of polydisperse mixtures.

References

[1] Rabe M, Verdes D and Seeger S 2011 Understanding protein adsorption phenomena at solid surfaces *Adv. Colloid Interface Sci.* **162** 87–106

[2] Ciesla M 2013 Continuum random sequential adsorption of polymer on a flat and homogeneous surface *Phys. Rev.* E **87** 052401

[3] Dabrowski A 2001 Adsorption from theory to practice *Adv. Colloid Interface Sci.* **93** 135–224

[4] Evans J W 1993 Random and cooperative sequential adsorption *Rev. Mod. Phys.* **65** 1281–329

[5] Talbot J, Tajrus G, Van Tassel P R and Viot P 2000 From car parking to protein adsorption: an overview of sequential adsorption process *Colloids Surf.* A **165** 287–324

[6] Privman V 2000 Dynamics of nonequilibrium deposition *Colloids Surf.* A **165** 231–40

[7] Cadilhe A, Araujo N A M and Privman V 2007 Random sequential adsorption: from continuum to lattice and pre-patterned substrates *J. Phys.: Condens. Matter* **19** 065124

[8] Bartelt M C and Privman V 1991 Kinetics of irreversible adsorption of mixtures of pointlike and fixed-size particles: exact results *Phys. Rev.* A **44** R2227–30

[9] Ben-Naim E and Krapivsky P L 1994 On irreversible deposition on disordered substrates *J. Phys. A: Math. Gen.* **27** 3575–7

[10] Cornette V, Linares D, Ramirez-Pastor A J and Nieto F 2007 Random sequential adsorption of polyatomic species *J. Phys. A: Math. Theor.* **40** 11765–76

[11] Ciesla M and Jakub Barbasz 2014 Random packing of regular polygons and star polygons on a flat two-dimensional surface *Phys. Rev.* E **90** 022402

[12] Budinski-Petković Lj, Lončarević I, Jakšić Z M, Vrhovac S B and Švrakić N M 2011 Simulation study of anisotropic random sequential adsorption of extended objects on a triangular lattice *Phys. Rev.* E **84** 051601

[13] Ciesla M, Pajk G and Ziff R M 2016 In a search for a shape maximizing packing fraction for two-dimensional random sequential adsorption *J. Chem. Phys.* **145** 044708

[14] Budinski-Petković Lj, Lončarevic I, Dujak D, Karač A, Šćepanović J R, Jakšić Z M and Vrhovac S B 2017 Particle morphology effects in random sequential adsorption *Phys. Rev.* E **95** 022114

[15] Garcia G D, Sanchez-Varretti F O, Centres P M and Ramirez-Pastor A J 2015 Random sequential adsorption of straight rigid rods on a simple cubic lattice *Physica* A **436** 558–64

[16] Staufer D and Aharony A 1994 *Introduction to Percolation Theory* (London: Taylor and Fransis)

[17] Kondrat G and Pekalski A 2001 Percolation and jamming in random sequential adsorption of linear segments on a square lattice *Phys. Rev.* E **63** 051108

[18] Rampf F and Albano E V 2002 Interplay between jamming and percolation upon random sequential adsorption of competing dimers and monomers *Phys. Rev.* E **66** 061106

[19] Adamczyk P, Romiszowski P and Sikorski A 2008 A simple model of stiff and flexible polymer chain adsorption: the influence of internal chain architecture *J. Chem. Phys.* **128** 154911

[20] Kondrat G 2002 Influence of temperature on percolation in a simple model of flexible chains adsorption *J. Chem. Phys.* **117** 6662

[21] Kondrat G 2008 Impact of composition of extended objects on percolation on a lattice *Phys. Rev.* E **78** 011101

[22] Budinski-Petković Lj, Lončarević I, Petković M, Jakšić Z M and Vrhovac S B 2012 Percolation in random sequential adsorption of extended objects on a triangular lattice *Phys. Rev.* E **85** 061117

[23] Kondrat G 2005 The study of percolation with the presence of impurities *J. Chem. Phys.* **122** 184718

[24] Budinski-Petković Lj, Lončarevic I, Jakšić Z and Vrhovac S 2016 Jamming and percolation in random sequential adsorption of extended objects on a triangular lattice with quenched impurities *J. Stat. Mech.* 053101

[25] Lončarević I, Dujak D, Jakšić Z M, Karač A, Budinski-Petković Lj and Vrhovac S B 2019 The study of tracer diffusion with the presence of extended obstacles *Physica* A **527** 121258

[26] Švrakić N M and Henkel M 1991 Kinetics of irreversible deposition of mixtures *J. Phys.* I **1** 791–5

[27] Lončarević I, Budinski-Petković Lj and Vrhovac S B 2007 Simulation study of random sequential adsorption of mixtures on a triangular lattice *Eur. Phys. J.* E **24** 19

[28] Budinski-Petković Lj, Vrhovac S B and Lončarević I 2008 Random sequential adsorption of polydisperse mixtures on discrete substrates *Phys. Rev.* E **78** 061603

[29] Lončarević I, Budinski-Petković Lj and Vrhovac S B 2007 Reversible random sequential adsorption of mixtures on a triangular lattice *Phys. Rev.* E **76** 031104

[30] Newman M E J and Ziff R M 2001 Fast Monte Carlo algorithm for site or bond percolation *Phys. Rev.* E **64** 016706